

# An in-depth analysis of the synchronization between the measured and predicted cutting forces for developing instantaneous milling force model

M. Wan\*, W.H. Zhang\*\*, G. Tan, G.H. Qin

*Sino-French Laboratory of Concurrent Engineering, The Key Laboratory of Contemporary Design & Integrated Manufacturing Technology, School of Mechatronic Engineering, Northwestern Polytechnical University, P.O. Box 552, 710072 Xi'an, Shaanxi, China*

Received 13 September 2006; received in revised form 14 January 2007; accepted 24 January 2007

Available online 12 February 2007

## Abstract

This paper proposes an analytical approach to synchronize the measured and predicted cutting forces for calibrating instantaneous cutting force coefficients that vary with the instantaneous uncut chip thickness in general end milling. Essential issues such as the synchronization criterion, phase determination of measured cutting forces, specification of calibration experiments and related cutting parameters are highlighted both theoretically and numerically to ensure the calibration accuracy. A closed-form criterion is established to select cutting parameters ensuring the single tooth engagement. Numerical cutting simulations and experimental test results are compared to validate the proposed approach.

© 2007 Elsevier Ltd. All rights reserved.

*Keywords:* Instantaneous cutting force coefficients; Synchronization; General end milling; Instantaneous uncut chip thickness; Cutting force model

## 1. Introduction

Milling is a commonly used process in manufacturing industry. Reliable prediction of milling forces is significant for the simulation of the machinability, cutter breakage, cutter wear, chatter and surface quality. Thus, much attention has been paid to the development of the cutting force model including the calibration of cutting force coefficients [1–9].

In general, two typical cutting force models exist: the lumped-mechanism force model [1–4] and the dual-mechanism force model [5–9]. The former combines the shearing effect on the rake face and the rubbing effect at the cutting edge into a single coefficient for each cutting force component along tangential, radial and axial directions, whereas the latter represents the shearing and rubbing effects with two independent coefficients. Within

this scope, a large amount of work has been carried out to calibrate the cutting force coefficients. A literature review shows that two basic calibration approaches are often used: a mechanistic modeling approach [1–4,7,9] and an orthogonal to oblique transformation approach [5]. Generally, both calibration procedures provide only one set of average cutting force coefficients from each cutting test. Hence, to obtain robust application range of the related cutting force model, a great number of cutting tests must be performed for different feeds, depths of cut, etc. These works are useful but in most cases the calibrated cutting force coefficients are only valid in the conditions under which the cutting tests are conducted. In addition, because the adopted cutting force coefficients are defined as a function of average uncut chip thickness or roughly as constants with statistical averaging, some prediction accuracy will be lost. For instance, Melkote and Endres [10] illustrated some disagreement between the predicted cutting forces and measured ones. This means that the cutting force coefficients must be modeled as varying parameters depending upon the instantaneous uncut chip thickness instead of being simply treated as constants or functions of

\*Corresponding author.

\*\*Also corresponding author. Tel./fax: +86 29 88495774

E-mail addresses: m.wan@nwpu.edu.cn (M. Wan), zhangwh@nwpu.edu.cn (W.H. Zhang).

average uncut chip thickness. As the cutter undergoes a trochoidal motion that yields a continuous variation of chip thickness from zero to maximum value, it would be possible to identify the instantaneous cutting force coefficients related to the instantaneous cutting forces over a wide range of chip thickness.

In fact, the concept of instantaneous cutting force coefficients has been introduced by many researchers, typically in [11–16] where the normal force coefficient  $K_n$ , the frictional force coefficient  $K_f$  and the chip flow angle  $\theta_c$  are used to characterize the lumped cutting force model. Cheng et al. [11] modeled the instantaneous cutting force coefficients in terms of the instantaneous uncut chip thickness, the spindle speed and the cutting edge length of face milling. Shin and Waters [12] proposed a method to determine the instantaneous cutting force coefficients from only a few designed cutting tests so that the experiment cost can be considerably reduced. Meanwhile, an improved simulation model of chip flow angle was given. Yucesan et al. [13] and Bayoumi et al. [14] developed a calibration procedure of instantaneous cutting force coefficients using both the instantaneous uncut chip thickness and the cutter rake angle. Based on above works [11–14], Ko et al. [15,16] proposed a systematic procedure to determine the instantaneous cutting force coefficients and the cutter runout parameters for flat end mill and ball end mill. Alternatively, Wan et al. [17] proposed a calibrated method for the instantaneous cutting force coefficients and the runout parameters in general end-milling process.

It must be emphasized that the calibration of the instantaneous cutting force coefficients relies on the phases of measured cutting forces that cannot be however obtained from the dynamometer. Obtaining the phase of a measured cutting force curve consists in determining the instantaneous rotation angle relative to the measured force magnitude at a specific sampled point. The phase acts as a reference to synchronize the measured cutting forces and the simulated ones in the calibration procedure. It can be considered as the criterion that the calibration procedure has to satisfy. Within this scope, Yun and Cho [18] proposed a synchronization procedure for flat end milling based on numerical simulations of varying the cutting force coefficients. In their procedure, the simulated cutter rotation angle associated with the peak value of cutting forces ( $F_Y$ ) was used as the reference phase. The similar synchronization was also realized for ball end milling [16].

The purpose of this paper is to develop a comprehensive synchronization methodology to calibrate the instantaneous cutting force coefficients and runout in general end-milling process. Unlike the method described in [18], the proposed methodology aims at revealing the characteristics of how the cutting force changes with respect to the variation of the cutting force coefficients. Firstly, a synchronization criterion is proposed based on the study of the cutting force coefficients that are assumed to be constant and instantaneous, respectively. Cutting conditions satisfying the proposed synchronization criterion are

suggested. With theoretical demonstrations and numerical simulations, it is shown that the proposed synchronization criterion is suitable to calibrate the instantaneous cutting force coefficients of any available cutting force models. Finally, comparisons of numerical simulations and experiment cutting tests are illustrated for different types of cutters to show the validity of the proposed method.

## 2. Cutting force modeling

### 2.1. Basic cutting force model

Fig. 1 shows the detailed geometry of a general end mill outer shape, which was introduced in [8,9]. A variety of end mill shapes can be defined by changing seven geometric parameters:  $D$ ,  $R$ ,  $R_r$ ,  $R_z$ ,  $\alpha$ ,  $\beta$  and  $H$ . For example, the cylindrical and ball end mills correspond to  $\{D, R, R_r, R_z, \alpha, \beta, H\} = \{D, 0, D/2, 0, 0, 0, H\}$  and  $\{D, D/2, 0, D/2, 0, 0, H\}$ , respectively. Besides, definitions of the cutting parameters in this work are also illustrated in Fig. 1. Here,  $R_a$  and  $R_w$  denote the real axial and radial depth of cut, respectively whereas  $R_{pa}$  is the pseudo axial depth of cut that is not engaged.  $R_{cut}$  is the maximum radius of the cutting edge point that is engaged with the workpiece. The cutter is divided into a finite number of disk elements along the cutter axis.

For the  $j$ th axial disk element of the  $i$ th flute, three orthogonal milling force components at an arbitrary cutter rotation angle  $\varphi$  can be expressed as [1–4]

$$\begin{aligned} F_{i,j,t}(\varphi) &= K_{i,j,t}(\varphi)h_{i,j}(\varphi)b_{i,j}, \\ F_{i,j,r}(\varphi) &= K_{i,j,r}(\varphi)h_{i,j}(\varphi)b_{i,j}, \\ F_{i,j,a}(\varphi) &= K_{i,j,z}(\varphi)h_{i,j}(\varphi)b_{i,j} \end{aligned} \quad (1)$$

with

$$\begin{aligned} h_{i,j}(\varphi) &= h_{i,j}^c \sin \kappa(z), \\ b_{i,j} &= z_{i,j} / \sin \kappa(z), \end{aligned} \quad (2)$$

where  $h_{i,j}(\varphi)$  and  $\kappa(z)$  are the instantaneous uncut chip thickness and the axial immersion angle related to the  $j$ th axial disk element of the  $i$ th flute at  $\varphi$ , respectively. Parameters  $K_{i,j,t}(\varphi)$ ,  $K_{i,j,r}(\varphi)$ ,  $K_{i,j,z}(\varphi)$  are the instantaneous cutting force coefficients corresponding to  $h_{i,j}(\varphi)$ .  $z$  and  $z_{i,j}$  are the axial coordinate and the axial length of the  $j$ th axial disk element of the  $i$ th flute, respectively.  $h_{i,j}^c$  is here named as instantaneous medial chip thickness corresponding to  $h_{i,j}(\varphi)$ .

At a certain location on the cutting edge,  $h_{i,j}^c$  can be approximated as [19–22]

$$h_{i,j}^c = m_i f_z \sin \phi_{i,j}(\varphi) + R_i(z) - R_{i-m_i}(z) \quad (3)$$

where  $f_z$  is the feed per tooth and  $m_i$  is the number indicating that the current tooth  $i$  is removing the material left by the  $m_i$ th previous tooth.  $\phi_{i,j}(\varphi)$  is the angular position of  $j$ th disk element of the  $i$ th flute at the current cutter rotation angle  $\varphi$ .  $R_i(z)$  is the actual cutting radius of the corresponding disk element involving the effect of the

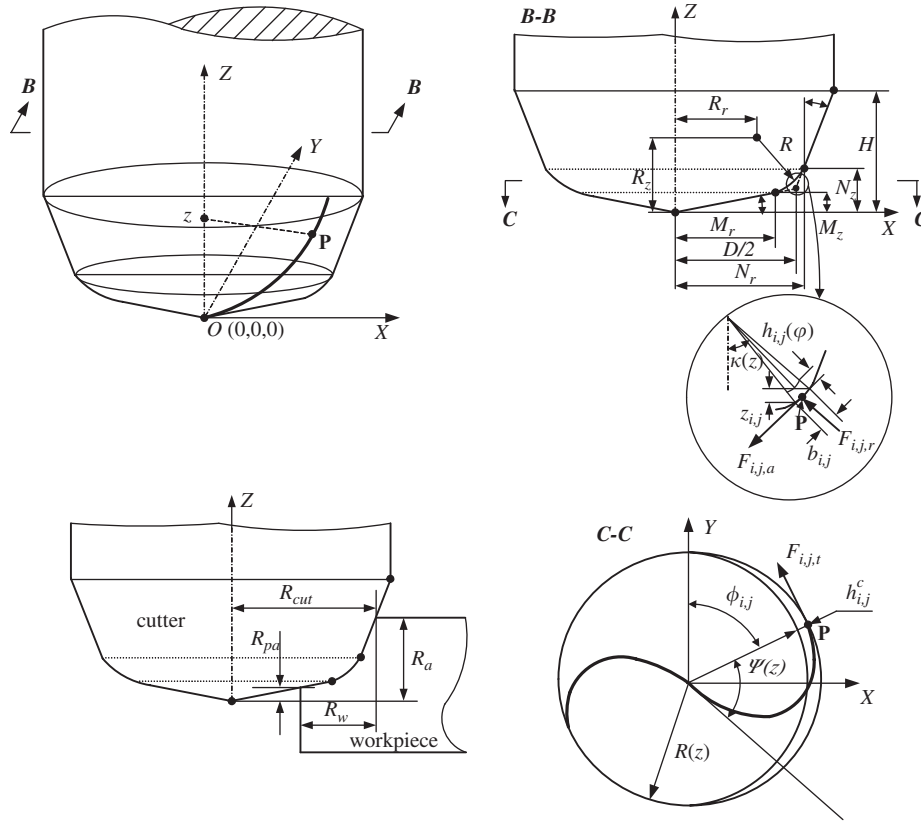


Fig. 1. Geometric model of a general end mill and cutting parameters.

cutter runout.  $R_i(z)$  will be calculated as [21,22]

$$R_i(z) = R(z) + \rho \cos[\lambda - \psi(z) - 2(i - 1)\pi/N], \quad (4)$$

where  $\rho$  and  $\lambda$  denote runout parameters.  $R(z)$  is the ideal cutting radius of the corresponding disk element.  $\psi(z)$  is the radial lag angle at  $z$  due to the cutter helix angle  $i_0$ .

Once three force components are obtained from Eq. (1), they can be mapped along  $X$ ,  $Y$  and  $Z$  directions [8,9]

$$\begin{aligned} \begin{bmatrix} F_{i,j,X}(\varphi) \\ F_{i,j,Y}(\varphi) \\ F_{i,j,Z}(\varphi) \end{bmatrix} &= \mathbf{T}_{i,j}(\varphi) \cdot \begin{bmatrix} F_{i,j,t}(\varphi) \\ F_{i,j,r}(\varphi) \\ F_{i,j,a}(\varphi) \end{bmatrix} \\ &= h_{i,j}^c \cdot z_{i,j} \cdot \mathbf{T}_{i,j}(\varphi) \cdot \begin{bmatrix} K_{i,j,t}(\varphi) \\ K_{i,j,r}(\varphi) \\ K_{i,j,z}(\varphi) \end{bmatrix} \end{aligned} \quad (5)$$

with

$$\mathbf{T}_{i,j}(\varphi) = \begin{bmatrix} -\cos \phi_{i,j}(\varphi) & -\sin \kappa(z) \sin \phi_{i,j}(\varphi) & -\cos \kappa(z) \sin \phi_{i,j}(\varphi) \\ \sin \phi_{i,j}(\varphi) & -\sin \kappa(z) \cos \phi_{i,j}(\varphi) & -\cos \kappa(z) \cos \phi_{i,j}(\varphi) \\ 0 & \cos \kappa(z) & -\sin \kappa(z) \end{bmatrix}. \quad (6)$$

Subsequently, the total cutting force components at any cutter rotation angle  $\varphi$  can be evaluated by summing the

forces acting on all flutes and disk elements.

$$F_s(\varphi) = \sum_{i,j} F_{i,j,s}(\varphi), \quad s = X, Y, Z. \quad (7)$$

## 2.2. Calibration of cutting force coefficients

For the specific cutter geometry, cutting conditions, workpiece material, milling forces together with the cutting force coefficients can be modeled using the experimental data. Conventionally, the cutting force coefficients are determined using measured average cutting forces. In most cases the identified coefficients are only valid in the range of the conditions under which the cutting tests are performed. To improve the applicability and prediction accuracy of the model, we propose here an alternative method that uses instantaneous values extracted from the measured data to calibrate the instantaneous cutting force coefficients  $K_{i,j,t}(\varphi)$ ,  $K_{i,j,r}(\varphi)$ ,  $K_{i,j,z}(\varphi)$ .

If the values of  $F_{i,j,X}(\varphi)$ ,  $F_{i,j,Y}(\varphi)$  and  $F_{i,j,Z}(\varphi)$  can be measured and the runout parameters  $\rho$  and  $\lambda$  are known in advance,  $K_{i,j,q}(\varphi)$  ( $q = t, r, z$ ) can be obtained from Eqs. (3) to (5). However, the measured cutting forces using dynamometer are available only in the form of total cutting forces  $F_s(\varphi)$  ( $s = X, Y, Z$ ) and cannot be decomposed into force components  $F_{i,j,X}(\varphi)$ ,  $F_{i,j,Y}(\varphi)$  and  $F_{i,j,Z}(\varphi)$ . At the same time, values of  $\rho$  and  $\lambda$  cannot be obtained

directly from the experiment. These make it practically impossible to establish ‘strict’ relationship between  $K_{i,j,q}(\varphi)$  and  $h_{i,j}(\varphi)$ . Therefore, an approximate approach is proposed below.

At the given cutting instant shown in Fig. 1,  $\phi_{i,j}(\varphi)$  refers to the angular position of the  $j$ th axial disk element of the  $i$ th flute. Obviously, after the cutter is rotated with an angle of  $(2k\pi)/N$  ( $k = 1, 2, \dots, N-1$ ), the angular position of the  $j$ th axial disk element of the  $(i+k)$ th flute equals  $\phi_{i,j}(\varphi)$ , too. If the cutting force coefficients are assumed to have the same values  $K_q(\varphi)$  ( $q = t, r, z$ ) at  $\varphi + (2k\pi)/N$  ( $k = 1, 2, \dots, N-1$ ), the sum of each  $X$ -,  $Y$ - and  $Z$ -force component of the cutter elements located at the angular position  $\phi_{i,j}(\varphi)$  over one rotation period corresponds to

$$\begin{bmatrix} F_{j,X}(\varphi) \\ F_{j,Y}(\varphi) \\ F_{j,Z}(\varphi) \end{bmatrix} = \begin{bmatrix} -\cos \phi_{i,j}(\varphi) & -\sin \kappa(z) \sin \phi_{i,j}(\varphi) & -\cos \kappa(z) \sin \phi_{i,j}(\varphi) \\ \sin \phi_{i,j}(\varphi) & -\sin \kappa(z) \cos \phi_{i,j}(\varphi) & -\cos \kappa(z) \cos \phi_{i,j}(\varphi) \\ 0 & \cos \kappa(z) & -\sin \kappa(z) \end{bmatrix} \begin{bmatrix} K_t(\varphi) \sum_{i=1}^N [h_{i,j}(\varphi) \cdot b_{i,j}] \\ K_r(\varphi) \sum_{i=1}^N [h_{i,j}(\varphi) \cdot b_{i,j}] \\ K_z(\varphi) \sum_{i=1}^N [h_{i,j}(\varphi) \cdot b_{i,j}] \end{bmatrix} \quad (8)$$

with

$$\begin{aligned} \sum_{i=1}^N [h_{i,j}(\varphi) b_{i,j}] &= z_{i,j} \{ N f_z \sin \phi_{i,j}(\varphi) \\ &+ \sum_{i=1}^N [R_i(z) - R_{i-m_i}(z)] \} = N z_{i,j} f_z \sin \phi_{i,j}(\varphi). \end{aligned} \quad (9)$$

Note that the effect of cutter radial runout on term  $\sum_{i=1}^N [h_{i,j}(\varphi) \cdot b_{i,j}]$  vanishes. This means that the sum of each of three force components of all cutting edge elements having the same angular position  $\phi_{i,j}(\varphi)$  is independent of the runout. By substituting Eq. (9) into Eq. (8), dividing Eq. (8) by  $N$ , and then summing along the cutter axis, we can obtain

$$\begin{bmatrix} \overline{F_X(\varphi)} \\ \overline{F_Y(\varphi)} \\ \overline{F_Z(\varphi)} \end{bmatrix} = f_z \cdot [\mathbf{T}_1(\varphi)] \cdot \begin{bmatrix} K_t(\varphi) \\ K_r(\varphi) \\ K_z(\varphi) \end{bmatrix}, \quad (10)$$

where

$$\mathbf{T}_1(\varphi) = \begin{bmatrix} -\sum_{i,j} (z_{i,j} B_2) & -\sum_{i,j} (C_1 B_1) & -\sum_{i,j} (C_2 B_1) \\ \sum_{i,j} (z_{i,j} B_1) & -\sum_{i,j} (C_1 B_2) & -\sum_{i,j} (C_2 B_2) \\ 0 & \sum_{i,j} [C_2 \sin \phi_{i,j}(\varphi)] & -\sum_{i,j} [C_1 \sin \phi_{i,j}(\varphi)] \end{bmatrix} \quad (11)$$

with  $B_1 = \sin^2 \phi_{i,j}(\varphi)$ ,  $B_2 = \sin \phi_{i,j}(\varphi) \cos \phi_{i,j}(\varphi)$ ,  $C_1 = z_{i,j} \sin \kappa(z)$ ,  $C_2 = z_{i,j} \cos \kappa(z)$ .

Denote  $F_s^M(\varphi)$  ( $s = X, Y, Z$ ) to be instantaneous values of measured cutting forces at  $\varphi$ .  $\overline{F_s(\varphi)}$  that is named nominal cutting force components can be obtained as

$$\overline{F_s(\varphi)} = \frac{1}{N} \sum_{i=1}^N [F_s^M(\varphi + 2(i-1)\pi/N)], \quad s = X, Y, Z \quad (12)$$

Therefore, the instantaneous values of  $K_q(\varphi)$  ( $q = t, r, z$ ) can be deduced immediately from Eq. (10) with known  $\overline{F_s(\varphi)}$ . In the above procedure, as  $K_q(\varphi)$  is a function of  $\varphi$  and takes the same value  $K_q(\varphi)$  ( $q = t, r, z$ ) at  $\varphi + (2k\pi)/N$ , this makes it possible to establish a concise formulation independent of the cutter runout in the calibration of  $K_q(\varphi)$ . Mathematically, at every specified  $\varphi$ , the instantaneous average chip thickness (IACT)  $\bar{h}(\varphi)$  corresponding to  $\overline{F_s(\varphi)}$  can be calculated by

$$\bar{h}(\varphi) = \frac{\sum_{i,j} [h_{i,j}(\varphi) \Delta \psi_{i,j} R(z)]}{\sum_{i,j} [\Delta \psi_{i,j} R(z)]}, \quad (13)$$

where  $\Delta \psi_{i,j}$  indicates the radial lag angle for the  $j$ th axial disk element of the  $i$ th flute due to the cutter helix angle  $i_0$ .

Note that  $h_{i,j}(\varphi)$  in Eq. (13) is calculated without runout because the latter vanishes in the calibration procedure of  $K_q(\varphi)$ . With discrete values of  $K_q(\varphi)$  and  $\bar{h}(\varphi)$ , the relationship between  $K_q(\varphi)$  and  $\bar{h}(\varphi)$  can be fitted. Thereafter, the runout parameters  $\rho$  and  $\lambda$  can be identified correspondingly [17].

Finally, to characterize the relationship between  $K_{i,j,q}(\varphi)$  and  $h_{i,j}(\varphi)$ , one can replace  $\bar{h}(\varphi)$  with  $h_{i,j}(\varphi)$  in the fitted mathematical expression for the calculation of  $K_{i,j,q}(\varphi)$  in terms of  $h_{i,j}(\varphi)$ . The validity of this approach is demonstrated with simulation and experiment tests in Section 4.

### 3. Synchronization of the measured cutting forces and predicted ones

Clearly, the computation of  $K_q(\varphi)$  from Eq. (10) not only relies on values of  $\mathbf{T}_1(\varphi)$  and  $F_s(\varphi)$  expressed in Eqs. (11) and (12) but also the involved instantaneous phase  $\varphi$ . However, the sampled data acquired by the dynamometer provide only values of  $F_s^M(\varphi)$  and the corresponding sampled time. How to obtain the proper phases of the sampled cutting forces becomes therefore a preoccupied issue for such a computation. One can imagine that some synchronization criterion should be established to identify the phases of the measured cutting forces. To do this, numerical approaches might be developed to determine the phase angles of the simulated cutting forces indirectly. It is well recognized that cutting force coefficients will change when different cutting materials are tested. This will generally lead to different cutting force curves even though the cutting parameters remain unchanged. However, if some points of the predicted cutting force curves only change their magnitudes without phase shift with respect to the variation of the cutting force coefficients,

these characteristic points associated with the simulated cutting forces can be used as the phase references of the measured data. Practically, as the cutting force curve varies periodically, the *maximum value* (MAV) and the *minimum value* (MIV) are easily identified from the measured signals. If only the magnitudes change without phase shift, these values can be adopted as reference points in the synchronization procedure. For example, in Fig. 2, the MAV of  $F_Y$  at  $\varphi_0$  changes without phase shift when different cutting force coefficients are used. In this case,  $\varphi_0$  can be then selected as synchronization reference. Obviously, the MAV of  $F_Y$  at  $\varphi_0$  means that  $F_Y(\varphi_0) \geq F_Y(\varphi)$  holds over a local range of  $\varphi_0 - \varepsilon \leq \varphi \leq \varphi_0 + \varepsilon$  with  $\varepsilon$  to be the prescribed tolerance. MIV of  $F_Y$  at  $\varphi_0$  means that  $F_Y(\varphi_0) \leq F_Y(\varphi)$  over  $\varphi_0 - \varepsilon \leq \varphi \leq \varphi_0 + \varepsilon$ . Hence, the values of  $F_Y$  at  $\varphi_0$ ,  $\varphi'_0$  and  $\varphi''_0$  shown in Fig. 2 can be treated as MAVs. The values of  $F_Y$  at  $\varphi^*$  and  $\varphi^{**}$  can be treated as MIVs whereas values of  $F_Y$  in the interval  $(\varphi^*, \varphi^{**})$  can be treated as MAVs or MIVs.

In the next section, numerical analyses and theoretical demonstrations will be given on how to figure out the synchronization no matter what the cutting force coefficients are.

### 3.1. Effects of cutting force coefficients upon cutting forces

#### 3.1.1. Numerical analysis

Without loss of generality, consider the cutting forces predicted by changing cutting force coefficients  $K_{i,j,q}(\varphi)$  ( $q = t, r, z$ ) of Eq. (7) for a four-fluted flat end mill in down milling. Firstly,  $K_{i,j,q}(\varphi)$  of each disk element are assumed to be constant values noted by  $K_q$  and two different sets of constant values are set to  $K_q$  as used in [18]. The predicted results of  $F_Y$  are shown in Figs. 3(a and b). Secondly,  $K_{i,j,q}(\varphi)$  are supposed to be instantaneous cutting force coefficients. A set of values is randomly set to  $K_{i,j,q}(\varphi)$  of

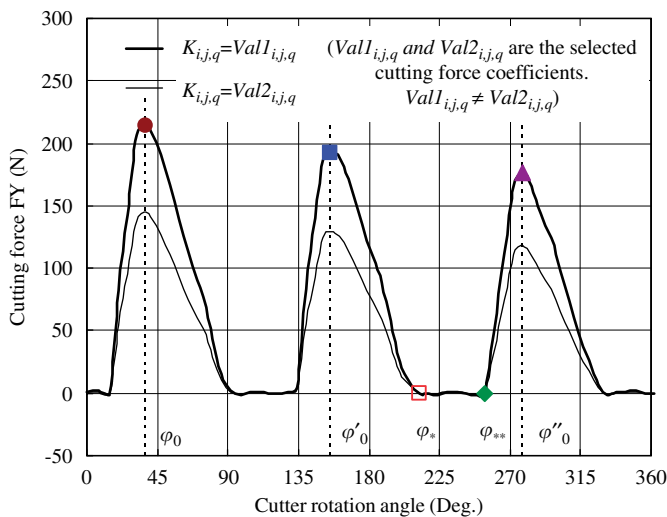


Fig. 2. Variations of cutting force  $F_Y$  due to the change of cutting force coefficients.

each disk element. Predicted results of  $F_Y$  are shown in Figs. 3(c and d). Note that the variation of  $K_{i,j,z}(\varphi)$  or  $K_z$  is here neglected due to its independence of  $F_Y$ .

It can be seen that multiple teeth engagement (MTE) occurs in Figs. 3(a and c) whereas the single tooth engagement (STE) retains always in Figs. 3(b and d). Intuitively, in the case of MTE, both MAV and MIV of  $F_Y$  have phase shifts with respect to the variation of cutting force coefficients. In the case of STE, certain MAVs or MIVs of  $F_Y$ , e.g., the values in the regions of  $\delta_1$ ,  $\delta_2$  and  $\delta_3$  illustrated in Fig. 3(b), have no phase shift when cutting force coefficients are changed. The similar phenomena can also be observed from the simulation results of  $F_X$  and  $F_Z$ . For  $F_Z$ , no phase shifts occur when cutting force coefficients are assumed to be constant in both MTE and STE, whereas only the zero values have no phase shift when cutting force coefficients are related to the instantaneous uncut chip thickness in STE. In summary, the above observations imply that *the cutting tests of STE can be used to calibrate the instantaneous cutting force coefficients because some values of the cutting forces, e.g., all values in  $\delta_1$ ,  $\delta_2$  and  $\delta_3$  shown in Fig. 3(b), can be selected as phase references for synchronization.* The same conclusions are also obtained from the simulations of  $F_X$ ,  $F_Y$  and  $F_Z$  in bull nose and ball end-milling process.

#### 3.1.2. Theoretical analysis

If the cutting force  $F_s(\varphi)$  takes the value of either MAV or MIV at the cutter rotation angle  $\varphi$ , the following relation holds

$$\frac{dF_s(\varphi)}{d\varphi} = 0. \quad (14)$$

By combining Eqs. (5) and (6), we can write

$$F_{i,j,Y}(\varphi) = \begin{bmatrix} A_{i,j}^{21}(\varphi) & A_{i,j}^{22}(\varphi) & A_{i,j}^{23}(\varphi) \end{bmatrix} \cdot \begin{bmatrix} K_{i,j,t}(\varphi) \\ K_{i,j,r}(\varphi) \\ K_{i,j,z}(\varphi) \end{bmatrix} \quad (15)$$

with

$$\begin{aligned} A_{i,j}^{21}(\varphi) &= h_{i,j}^c z_{i,j} \sin \phi_{i,j}(\varphi), \\ A_{i,j}^{22}(\varphi) &= -h_{i,j}^c z_{i,j} \sin \kappa(z) \cos \phi_{i,j}(\varphi), \\ A_{i,j}^{23}(\varphi) &= -h_{i,j}^c z_{i,j} \cos \kappa(z) \cos \phi_{i,j}(\varphi). \end{aligned} \quad (16)$$

*Case I:* If the cutting force coefficients are assumed to be functions of the instantaneous uncut chip thickness associated with each disk elements and symbolized as  $K_{i,j,q}(\varphi)$ ,  $F_Y(\varphi)$  can be expressed as

$$\begin{aligned} F_Y(\varphi) &= \sum_{i,j} (K_{i,j,t}(\varphi) A_{i,j}^{21}(\varphi)) + \sum_{i,j} (K_{i,j,r}(\varphi) A_{i,j}^{22}(\varphi)) \\ &+ \sum_{i,j} (K_{i,j,z}(\varphi) A_{i,j}^{23}(\varphi)). \end{aligned} \quad (17)$$

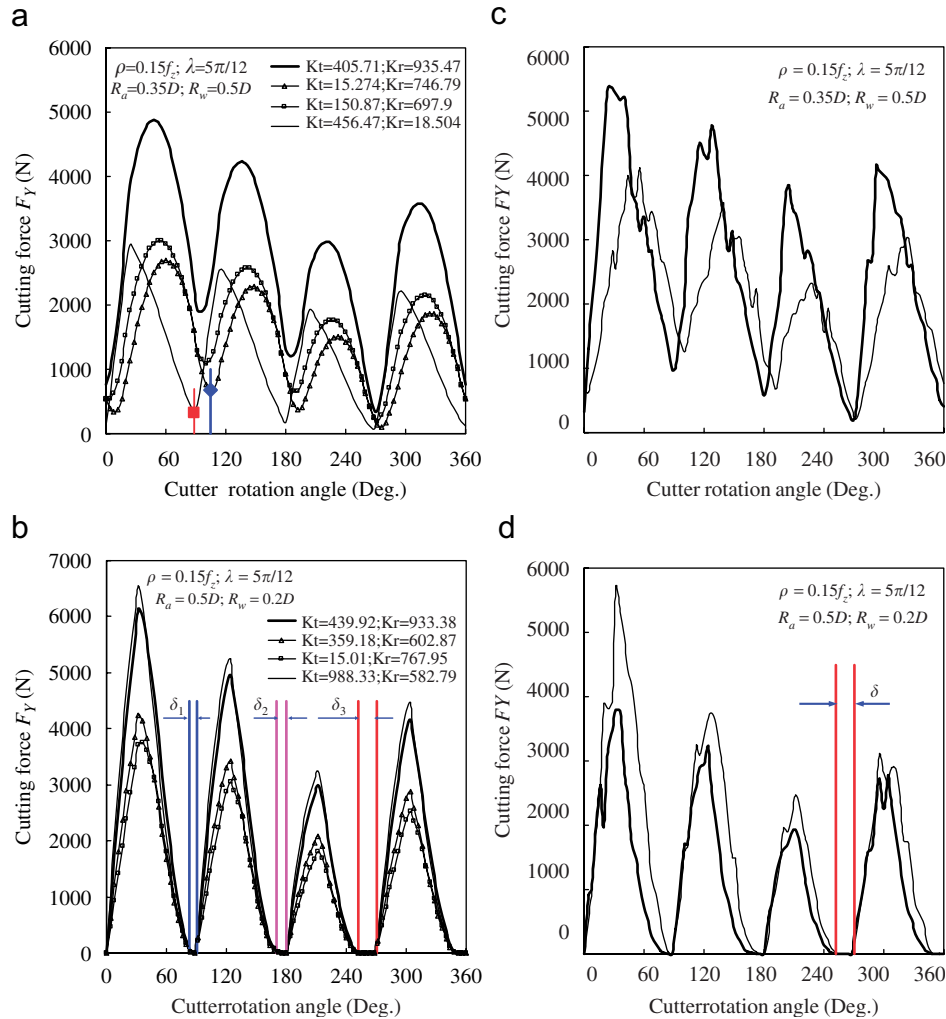


Fig. 3. Simulations of cutting forces with the variation of cutting force coefficients: (a) the case of MTE with constant cutting force coefficients  $K_q$ ; (b) the case of STE with constant cutting force coefficients  $K_q$ ; (c) the case of MTE with instantaneous cutting force coefficients  $K_{i,j,q}(\varphi)$  and (d) the case of STE with instantaneous cutting force coefficients  $K_{i,j,q}(\varphi)$ .

Applying Eq. (14) to Eq. (17), one can obtain

$$\sum_{ij} \left[ \frac{dA_{ij}^{21}(\varphi)}{d\varphi} K_{ij,t}(\varphi) \right] + \sum_{ij} \left[ \frac{dA_{ij}^{22}(\varphi)}{d\varphi} K_{ij,r}(\varphi) \right] + \sum_{ij} \left[ \frac{dA_{ij}^{23}(\varphi)}{d\varphi} K_{ij,z}(\varphi) \right] = 0. \quad (18)$$

To hold the above equation for arbitrary  $K_{i,j,q}(\varphi)$ , it is required for all disk elements that

$$\frac{dA_{ij}^{21}(\varphi)}{d\varphi} = 0, \quad \frac{dA_{ij}^{22}(\varphi)}{d\varphi} = 0, \quad \frac{dA_{ij}^{23}(\varphi)}{d\varphi} = 0. \quad (19)$$

Besides, if the cutting test is designed like that in Fig. 3(d), there exist some cutter rotation angle regions, e.g.,  $\delta$  in which no flutes are engaged with the workpiece. When the third tooth disengages from the workpiece, the fourth one in Fig. 3(d) will be engaged with the workpiece after some cutter rotation angles. Obviously, in the region

of  $\delta$ , we have  $h_{ij}^c \equiv 0$ . This will lead to  $A_{ij}^{2k}(\varphi) \equiv 0$  ( $k = 1, 2, 3$ ) defined in Eq. (16) and hence  $dA_{ij}^{2k}(\varphi)/d\varphi = 0$ . Therefore, in the case of STE, if specific regions of cutter rotation angles exist such as  $\delta (> 0)$  in Fig. 3(d), Eq. (18) will be automatically satisfied in  $\delta$  no matter how the cutting force coefficients vary.

Case II: If the cutting force coefficients are supposed to be constants  $K_q$  irrespective of the instantaneous uncut chip thickness,  $F_Y(\varphi)$  can be expressed as

$$F_Y(\varphi) = \left[ \sum_{ij} A_{ij}^{21}(\varphi) \quad \sum_{ij} A_{ij}^{22}(\varphi) \quad \sum_{ij} A_{ij}^{23}(\varphi) \right] \cdot \begin{bmatrix} K_t \\ K_r \\ K_z \end{bmatrix} = [A21(\varphi) \quad A22(\varphi) \quad A23(\varphi)] \cdot \begin{bmatrix} K_t \\ K_r \\ K_z \end{bmatrix} \quad (20)$$

which is just a particular case of Eq. (17).

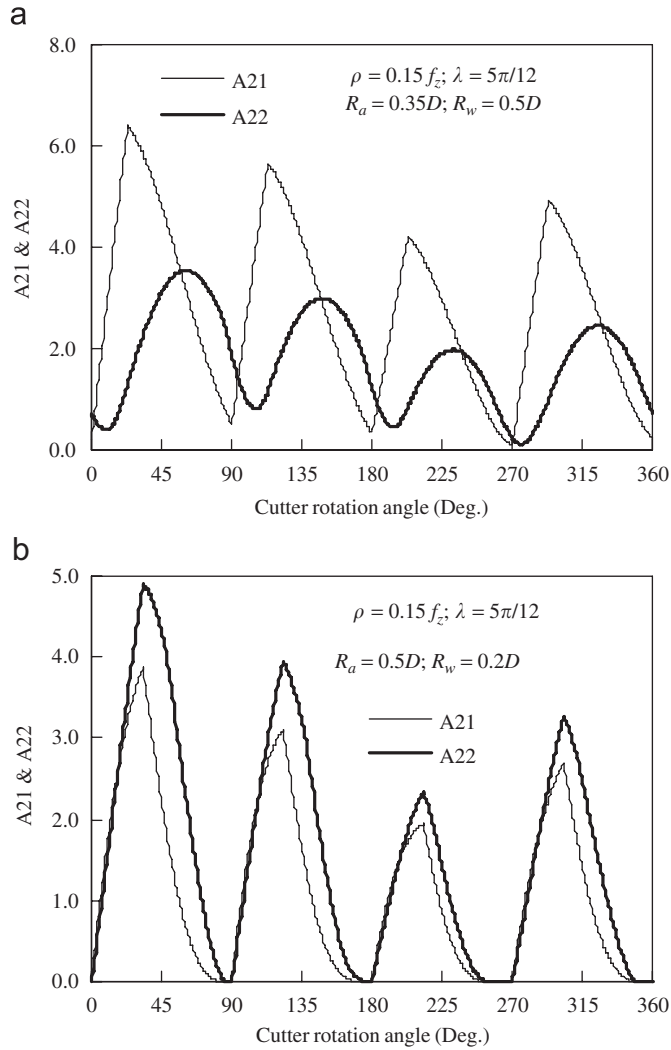


Fig. 4. The variation of A21 and A 22 in flat end milling: (a) the case of MTE and (b) the case of STE.

Similarly to the above analysis,  $A2k(\varphi) \equiv 0$  ( $k = 1, 2, 3$ ) in regions  $\delta_1$ ,  $\delta_2$  and  $\delta_3$  of Fig. 3(b). Fig. 4 shows the variations of  $A2k(\varphi)$  versus the cutter rotation angles for a flat end-milling process when the same cutting conditions used in Fig. 3 are applied. In case of STE shown in Fig. 4, the fact that  $A2k(\varphi) \equiv 0$  only appears in the specific cutter rotation angle regions just confirms the phenomena occurring in Fig. 3(b). It should be noted that in the flat end-milling process,  $F_Z$  is expressed as

$$F_Z(\varphi) = -K_z \sum_{i,j} [h_{i,j}^c z_{i,j}]. \quad (21)$$

As  $F_Z(\varphi)$  varies proportionally with  $K_z$ , all values of  $F_Z(\varphi)$  have always no phase shift in flat end milling as described in Section 3.1.

Therefore, in both cases, the phases  $\varphi$  in  $\delta$  can be adopted as synchronization reference as long as  $\delta$  exists in the designed STE cutting tests. Based on Eq. (14), similar analyses of  $F_X$  and  $F_Z$  show that only the phase angle in  $\delta$  can be selected as phase reference for synchronization in

the case of STE. Generally, for a  $N$ -fluted mill, one can select the right extreme point  $2k\pi/N$  ( $k = 0, 1, \dots, N-1$ ), that corresponds to the zero value of the cutting force in the case of STE. Now the problem is how to realize the STE cutting state ensuring the existence of  $\delta$ .

### 3.2. Selection of cutting parameters

In fact, the STE can be easily satisfied with a reasonable selection of the radial depth of cut,  $R_w$  and axial depth of cut,  $R_a$ . Critical values of  $R_w$  and  $R_a$  can be defined by the following cutting conditions: whenever the current tooth disengages from the workpiece, the next tooth has to be engaged with the workpiece immediately. This means that with critical  $R_a$  and  $R_w$ , any increase of  $R_w$  or  $R_a$  will lead to an engagement of at least two teeth simultaneously at some cutter rotation angles. Therefore, the STE retains at any time provided that

$$\psi(R_a) - \psi(R_{pa}) + \frac{\pi}{2} + \arcsin\left(\frac{R_w - R_{cut}}{R_{cut}}\right) < \frac{2\pi}{N}, \quad (22)$$

where  $\psi(R_a)$  indicates the radial lag angle corresponding to the axial depth of cut,  $R_a$ , due to the cutter helix angle  $i_0$ .

This is the critical condition characterizing the dependence between critical values of  $R_a$  and  $R_w$ . A non-zero  $\delta$  must exist as long as Eq. (22) is strictly satisfied. Critical conditions are now illustrated for a three-fluted flat end mill, three-fluted bull nose end mill and four-fluted ball end mill in Figs. 5(a–c).

Eq. (22) can be applied to design the experimental setup for calibration of instantaneous cutting force coefficients. If the measured signals of the cutting forces are not bright enough to identify  $\delta$  easily, we can appropriately reduce values of  $R_a$  or  $R_w$  until  $\delta$  appears clearly.

However, one must keep in mind that Eq. (22) is derived with the negligence of the cutter runout. Practically, if one tooth is engaged in cut with an immersed axial length more than its nominal value due to runout, there must be at least another tooth that will be in cut with an immersed axial length less than its nominal value after some cutter rotation angles. As a result, there must exist at least one non-zero region  $\delta$ . Therefore, as long as  $R_a$  and  $R_w$  satisfy Eq. (22), the cutting test is in the state of STE regardless of the cutter runout.

### 3.3. The whole calibrating procedure

The whole solution procedure of calibrating the cutting force coefficients and runout is summarized in Fig. 6. Firstly, the cutting parameters that satisfy the STE condition are selected. Secondly, the cutting forces are measured using the dynamometer, and the sampled points in one cutter rotation period are noted as  $Q_1, Q_2, Q_3, \dots, Q_i, \dots, Q_m$ . Thirdly, if  $Q_i$  is the right extreme point of one nonzero region  $\delta$ ,  $2k\pi/N$  is attributed as the reference phase of  $Q_i$ . Subsequently, by setting  $2k\pi/N \pm 2j\pi/(m-1)$  as the phase  $\varphi$  of all remaining sampled points  $Q_{i \pm j}$ , the

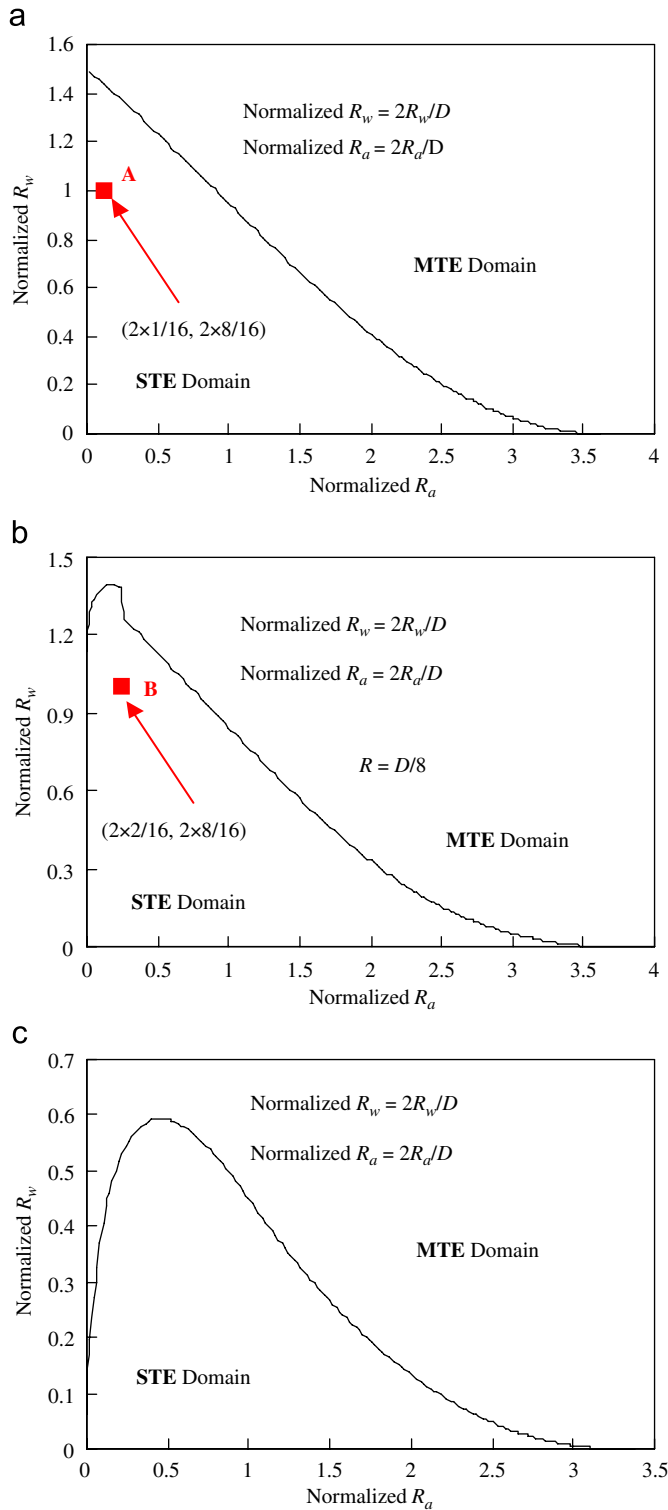


Fig. 5. Critical curves describing the engagement of a single flute: (a) three-fluted flat end mill with a helix angle of 30°; (b) three-fluted bull nose end mill with a helix angle of 30°; (c) four-fluted ball end mill with a helix angle of 35°.

synchronization is completed. Fourthly, the cutting force coefficients are calibrated by means of Eq. (10). Finally, the discretized cutting force coefficients obtained from Eq. (10) are fitted approximately.

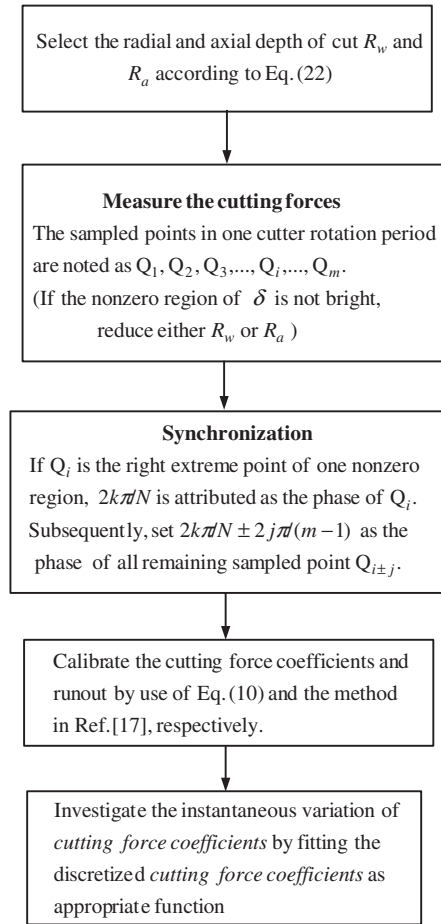


Fig. 6. The routine to calibrate the instantaneous cutting force coefficients and runout.

In fact, the proposed synchronization procedure has its generality of being applied to other cutting force models. In this sense, it is necessary to mention the cutting force model using the cutting force coefficients ( $K_n, K_f, \theta_c$ ) and studied by Cho and Altintas et al. [13,15,16]. The X-, Y- and Z-cutting force components acting on the  $j$ th axial disk element of the  $i$ th flute at the cutter rotation angle  $\varphi$  are expressed as

$$\begin{bmatrix} F_{i,j,X}(\varphi) \\ F_{i,j,Y}(\varphi) \\ F_{i,j,Z}(\varphi) \end{bmatrix} = \mathbf{T}_{CA}(\varphi) \cdot \begin{bmatrix} K_{i,j,1} \\ K_{i,j,2} \\ K_{i,j,3} \end{bmatrix} \quad (23)$$

where  $\mathbf{T}_{CA}(\varphi) = \begin{bmatrix} B_{i,j}^{11}(\varphi) & B_{i,j}^{12}(\varphi) & B_{i,j}^{13}(\varphi) \\ B_{i,j}^{21}(\varphi) & B_{i,j}^{22}(\varphi) & B_{i,j}^{23}(\varphi) \\ B_{i,j}^{31}(\varphi) & B_{i,j}^{32}(\varphi) & B_{i,j}^{33}(\varphi) \end{bmatrix}$  denotes the

parameters matrix depending upon not only  $\varphi$  but also cutter geometry and cutting parameters.  $K_{i,j,1}, K_{i,j,2}$  and  $K_{i,j,3}$  are the cutting force coefficients transformed from  $K_n, K_f, \theta_c$ . One can refer to Refs. [15,16] for the detailed computing of  $T_{CA}(\varphi), K_{i,j,1}, K_{i,j,2}$  and  $K_{i,j,3}$ .

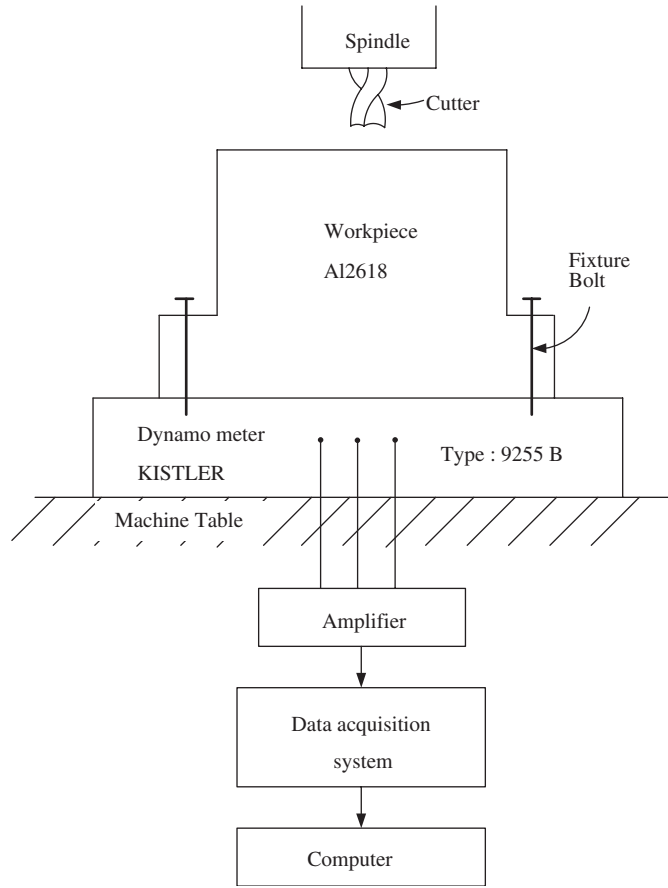


Fig. 7. Schematic figure of experiment set-up.

Table 1  
Geometry of mills

End mill	$D$ (mm)	$R$ (mm)	$R_r$ (mm)	$R_z$ (mm)	$\alpha$ (deg)	$\beta$ (deg)	$i_0$ (deg)
Flat	16	0	8	0	0	0	30
Bull nose	16	2	6	2	0	0	30

Table 2  
Cutting conditions

Cutter type	Test no.	Milling type	Radial depth of cut $R_w$ (mm)	Axial depth of cut $R_a$ (mm)	Feed per tooth $f_z$ (mm/tooth)	RPM
Flat	1	Down	8	1	0.05	2000
	2	Down	8	1.3	0.1	5000
	3	Down	3	8	0.0667	3000
	4	Up	3	6	0.05	2000
	5	Up	8	0.85	0.05	2000
	6	Slotting	16	2	0.05	3000
Bull nose	7	Down	8	2	0.05	2000
	8	Down	8	2.3	0.05	2000
	9	Down	8	2	0.1	5000
	10	Down	3	6	0.05	2000
	11	Up	8	2	0.05	2000
	12	Slotting	16	2	0.05	3000

Now, let us perform the analysis of  $F_Y(\varphi)$  that is expressed as

$$F_Y(\varphi) = \sum_{ij} [K_{i,j,1} B_{ij}^{21}(\varphi)] + \sum_{ij} [K_{i,j,2} B_{ij}^{22}(\varphi)] + \sum_{ij} [K_{i,j,3} B_{ij}^{23}(\varphi)]. \quad (24)$$

The form is very similar to Eq. (17) except the coefficient definitions of  $A_{ij}^{**}$  and  $B_{ij}^{**}$ .

According to the same analysis procedure described in Section 3.1.2, we can find such a  $\delta$  region in which the following relation holds in case of STE

$$B_{ij}^{21}(\varphi) = B_{ij}^{22}(\varphi) = B_{ij}^{23}(\varphi) \equiv 0. \quad (25)$$

As to the dual-mechanism cutting force model mentioned in [5,9], the  $X$ -,  $Y$ - and  $Z$ -cutting force components acting on the  $j$ th axial disk element of the  $i$ th flute at  $\varphi$  can be expressed as

$$\begin{bmatrix} F_{ij,X}(\varphi) \\ F_{ij,Y}(\varphi) \\ F_{ij,Z}(\varphi) \end{bmatrix} = \mathbf{T}_C(\varphi) \cdot \begin{bmatrix} K_{ij,tc} \\ K_{ij,rc} \\ K_{ij,zc} \end{bmatrix} + \mathbf{T}_E(\varphi) \cdot \begin{bmatrix} K_{ij,te} \\ K_{ij,re} \\ K_{ij,ze} \end{bmatrix}, \quad (26)$$

with

$$\mathbf{T}_C(\varphi) = \begin{bmatrix} C_{ij}^{11}(\varphi) & C_{ij}^{12}(\varphi) & C_{ij}^{13}(\varphi) \\ C_{ij}^{21}(\varphi) & C_{ij}^{22}(\varphi) & C_{ij}^{23}(\varphi) \\ C_{ij}^{31}(\varphi) & C_{ij}^{32}(\varphi) & C_{ij}^{33}(\varphi) \end{bmatrix}$$

and

$$\mathbf{T}_E(\varphi) = \begin{bmatrix} E_{ij}^{11}(\varphi) & E_{ij}^{12}(\varphi) & E_{ij}^{13}(\varphi) \\ E_{ij}^{21}(\varphi) & E_{ij}^{22}(\varphi) & E_{ij}^{23}(\varphi) \\ E_{ij}^{31}(\varphi) & E_{ij}^{32}(\varphi) & E_{ij}^{33}(\varphi) \end{bmatrix}$$

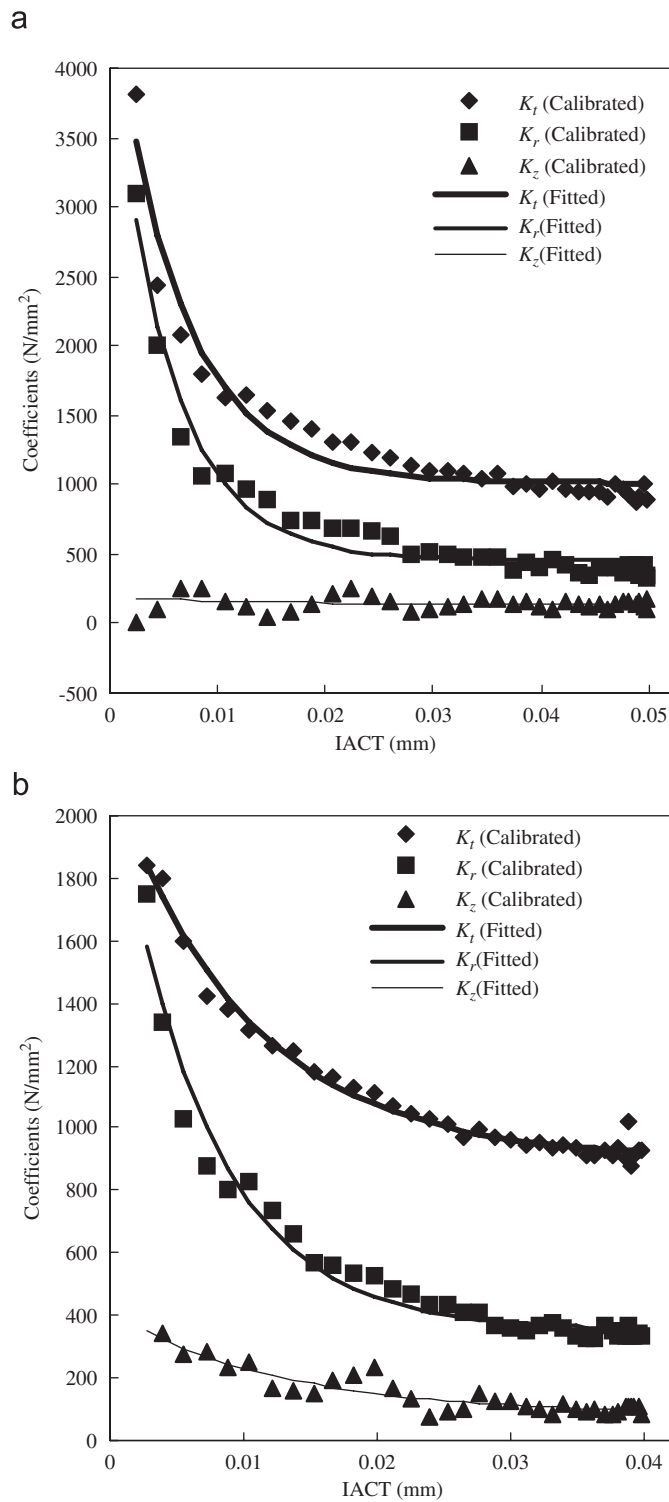


Fig. 8. Calibrated cutting force coefficients: (a) cutting force coefficients calibrated from Test 1 for flat end mill and (b) cutting force coefficients calibrated from Test 7 for bull nose end mill.

Note that  $K_{i,j,tc}$ ,  $K_{i,j,rc}$ ,  $K_{i,j,zc}$  and  $K_{i,j,te}$ ,  $K_{i,j,re}$ ,  $K_{i,j,ze}$  are the cutting force coefficients related to each instantaneous uncut chip thickness. Subsequently,  $F_Y(\varphi)$  can be

obtained as

$$F_Y(\varphi) = \sum_{ij} [K_{i,j,tc} C_{ij}^{21}(\varphi)] + \sum_{ij} [K_{i,j,rc} C_{ij}^{22}(\varphi)] + \sum_{ij} [K_{i,j,zc} C_{ij}^{23}(\varphi)] + \sum_{ij} [K_{i,j,te} E_{ij}^{21}(\varphi)] + \sum_{ij} [K_{i,j,re} E_{ij}^{22}(\varphi)] + \sum_{ij} [K_{i,j,ze} E_{ij}^{23}(\varphi)]. \quad (27)$$

Similarly, it concludes from Eq. (14) that a  $\delta$  region of cutter rotation angle exists provided that the following equations must hold

$$C_{ij}^{21}(\varphi) = C_{ij}^{22}(\varphi) = C_{ij}^{23}(\varphi) = E_{ij}^{21}(\varphi) = E_{ij}^{22}(\varphi) = E_{ij}^{23}(\varphi) \equiv 0. \quad (28)$$

The same analysis can also be performed for  $F_X$  and  $F_Z$  to find corresponding  $\delta$  regions. Actually, if the test is designed as STE based on Eq. (22), there are some cutter rotation angle regions in which no flutes are in cut. As a result, the cutting force values are always zero in these regions no matter what cutting force model is adopted. Accordingly, any phase, e.g.  $2\pi/N$ , in these regions can be used as reference for synchronization. Therefore, the STE verifying Eq. (22) is valid for the synchronization of all cutting force models.

#### 4. Test applications

To apply the above procedure, a series of cutting tests are performed in milling aluminum alloy 2618 with a vertical CNC milling machine. The experiment setup is illustrated schematically in Fig. 7. Three-component dynamometer Kistler 9255B is used to measure the cutting forces. The sampling rate is set to be 5000 Hz. The workpiece is connected to the dynamometer by four bolts. A three-fluted carbide flat end mill and a three-fluted carbide bull nose end mill are studied, respectively. Cutter geometries and cutting condition parameters are given in Tables 1 and 2, respectively. All tests are realized without coolant. As shown in Figs. 5(a and b), the combinations of  $R_w$  and  $R_a$  in Tests 1 and 7 correspond to points A and B that satisfy Eq. (22). Therefore, Tests 1 and 7 can be used to calibrate the cutting force coefficients as well as the runout parameters. Using the experiment condition data given above, the number of sampling points in one cutter rotation period is evaluated to be 151. In this work, the synchronization is based on the force component  $F_Y$  whose signals are more easily identified than those of  $F_X$  and  $F_Z$ . The synchronization procedure is completed according to the routine shown in Fig. 6.

Subsequently, with the aid of Eq. (10), the identified cutting force coefficients are plotted versus the instantaneous average chip thickness (IACT)  $\bar{h}(\varphi)$  in Fig. 8.

In Fig. 8, we can see that an exponent-like relation exists between cutting force coefficients  $K_q(\varphi)$  and  $\bar{h}(\varphi)$ . For this

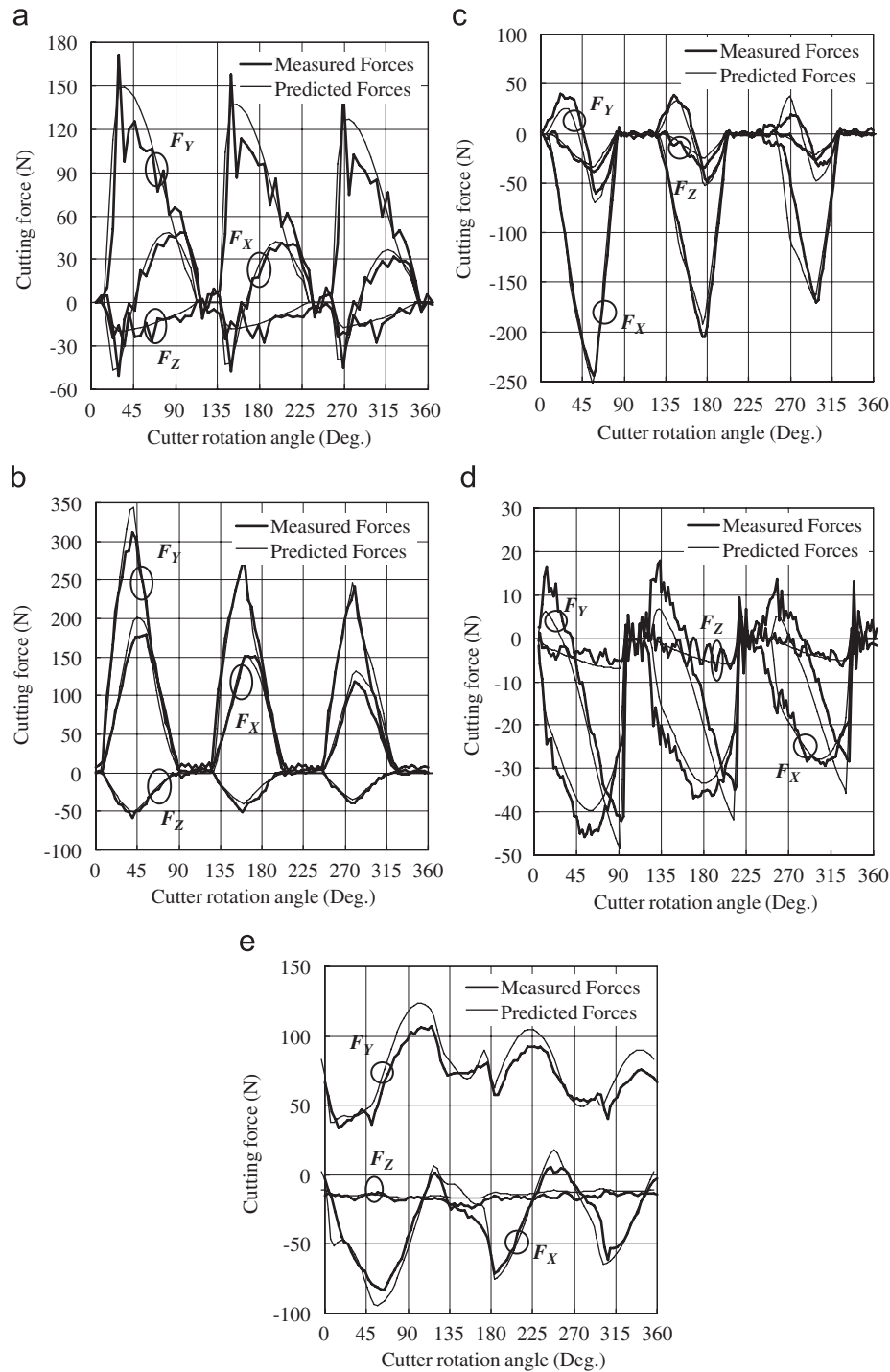


Fig. 9. Comparison of measured and predicted cutting forces for flat end mill: (a) Test 2; (b) Test 3; (c) Test 4; (d) Test 5 and (e) Test 6.

reason, the relationship between  $K_q(\varphi)$  and  $\tilde{h}(\varphi)$  is interpolated by the following nonlinear fitting function:

$$K_q(\varphi) = W_{q1} + W_{q2} \cdot e^{[W_{q3} \cdot \tilde{h}(\varphi)]} \quad (q = t, r, z). \quad (29)$$

The fitted cutting force coefficients are also illustrated in Fig. 8 for comparison with calibrated discrete values.

With fitted values of  $K_q(\varphi)$ , runout parameters  $\rho$  and  $\lambda$  are then identified by means of the approach described in Ref. [17]. Results are:

(I) flat end mill for Test 1

$$\rho_f = 5 \mu\text{m}, \quad \lambda_f = 60^\circ, \quad (30)$$

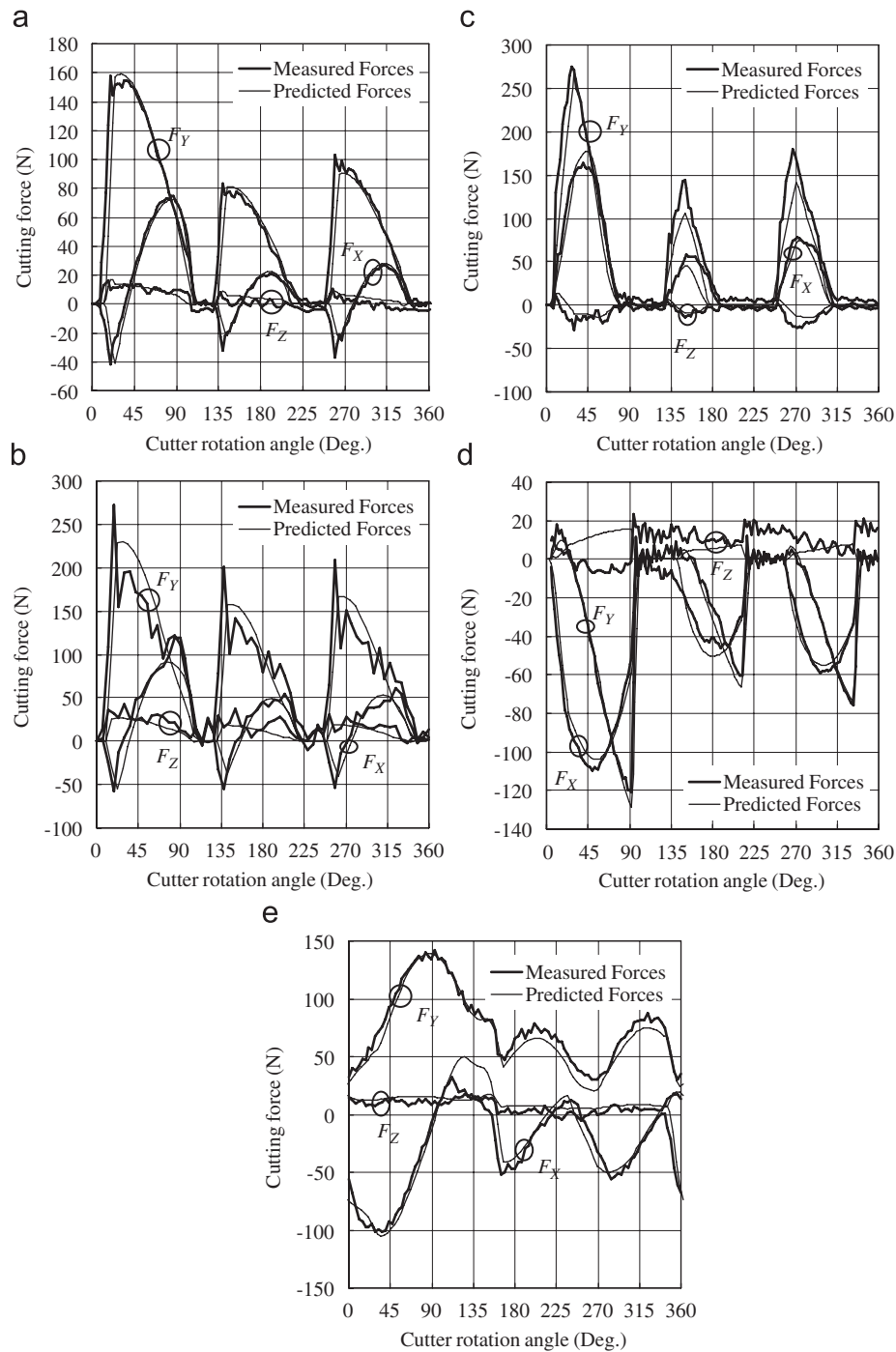


Fig. 10. Comparison of measured and predicted cutting forces for bull nose end mill: (a) Test 8; (b) Test 9; (c) Test 10; (d) Test 11 and (e) Test 12.

(II) bull nose end mill for Test 7  
 $\rho_b = 14 \mu\text{m}$ ,  $\lambda_b = 28^\circ$ . (31)

Now, remaining cutting Tests 2–6 and Tests 8–12 are used to verify the accuracy of calibrated cutting force model for flat end mill and bull nose end mill, respectively. To this end, fitted values of  $K_q(\varphi)$  in Eq. (29) are adopted. To characterize the relationship between  $K_{i,j,q}(\varphi)$  and the instantaneous uncut chip thickness of every axial disk

element, we can replace  $\bar{h}(\varphi)$  with  $h_{i,j}(\varphi)$  in Eq. (29) for calculation of  $K_{i,j,q}(\varphi)$ . This relationship is used for the numerical simulations through all cutting tests given below.

The predicted and measured cutting forces are compared in Figs. 9 and 10 for two types of cutters, respectively. Different cutting types are selected to validate the calibrated cutting force coefficients. In Figs. 9(a, b) and 10(a–c), the predicted and measured results are compared for down milling. In Figs. 9(c, d) and 10(d), the predicted

and measured results are compared for up milling. The comparison is also made in Fig. 9(e) and 10(e) for slotting milling. The variations of depths of cut, feed rate and cutting speed are also considered in these comparisons. It can be seen that a good agreement exists both in magnitude and in distribution no matter what cutting types and cutting conditions are, although the cutting coefficients are determined using only one cutting test. Therefore, the proposed methodology is not only general but also beneficial in saving the cost of cutting calibration tests.

## 5. Conclusions

A systematic methodology is proposed in this paper to synchronize the measured and the predicted cutting forces for calibrating the instantaneous cutting force coefficients. A generic synchronization criterion suitable to any available cutting force models in general end-milling process is developed. The advantage of the proposed methodology lies in that the synchronization criterion is introduced from both the strict theoretical analysis and the numerical simulation. Reasonable cutting parameters are provided to satisfy the synchronization criterion. It is found that:

- (1)  $2k\pi/N$  can be adopted as phase references for synchronization irrespective of the cutting force models as long as the cutting test is in STE.
- (2) The relationship between the instantaneous cutting force coefficients and the instantaneous uncut chip thickness can be established by fitting the discretized values of the coefficients that are calibrated directly from the measured data as function of the IACT of the whole cutter. Then, instantaneous uncut chip thickness of every separate disk element can be substituted into the fitted function for calculating the instantaneous cutting force coefficients associated with every single disk element. A variety of test cases are studied both numerically and experimentally. The comparison of simulation and experiment cutting forces demonstrates that the proposed methodology is validity and that the cutting force coefficients calibrated in STE can be also applied in MTE.

## Acknowledgments

This work is supported by the Doctorate Creation Foundation of Northwestern Polytechnical University (Grant No. CX200411), the Youth for NPU Teachers Scientific and Technological Innovation Foundation, the Natural Science Foundation of Shaanxi Province (Grant No. 2004E<sub>2</sub>17) and the 111Project (Grant No. B070050).

## References

- [1] W.A. Kline, R.E. DeVor, J.R. Lindberg, The prediction of cutting forces in end milling with application to cornering cuts, *Int J Mach Tool Des Res* 22 (1982) 7–22.
- [2] Y. Altintas, A. Spence, End milling force algorithms for CAD systems, *Ann CIRP* 40 (1) (1991) 31–34.
- [3] H.Y. Feng, N. Su, A mechanistic cutting force model for 3D ball-end milling, *Trans ASME J Manuf Sci Eng* 123 (2001) 23–29.
- [4] H.Y. Feng, C.H. Menq, The prediction of the cutting forces in the ball-end milling process-I. Model of formulation and model building procedure, *Int J Mach Tools Manuf* 34 (1994) 697–710.
- [5] E. Budak, Y. Altintas, E.J.A. Armarego, Prediction of milling force coefficients from orthogonal cutting data, *Trans ASME J Manuf Sci Eng* 118 (1996) 216–224.
- [6] Y. Altintas, P. Lee, Mechanics and dynamics of ball end milling, *Trans ASME J Manuf Sci Eng* 120 (1998) 684–692.
- [7] B. Ozturk, I. Lazoglu, H. Erdim, Machining of free-form surfaces, Part II: calibration and forces, *Int J Mach Tools Manuf* 46 (2006) 736–746.
- [8] S. Engin, Y. Altintas, Mechanics and dynamics of general milling cutters—Part I: helical end mills, *Int J Mach Tools Manuf* 41 (2001) 2195–2212.
- [9] J. Gradišek, M. Kalveram, K. Weinert, Mechanistic identification of specific force coefficients for a general end mill, *Int J Mach Tools Manuf* 44 (2004) 401–414.
- [10] S.N. Melkote, W.J. Endres, The importance of including size effect when modeling slot milling, *Trans ASME J Manuf Sci Eng* 120 (1998) 68–75.
- [11] P.J. Cheng, J.T. Tsay, S.C. Lin, A study on instantaneous cutting force coefficients in face, *Int J Mach Tools Manuf* 37 (1997) 1393–1408.
- [12] Y.C. Shin, A.J. Waters, A new procedure to determine instantaneous cutting force coefficients for machining force prediction, *Int J Mach Tools Manuf* 37 (1997) 1337–1351.
- [13] G. Yucesan, Y. Altintas, Improved modeling of cutting force coefficients in peripheral milling, *Int J Mach Tools Manuf* 34 (1994) 473–487.
- [14] A.E. Bayoumi, G. Yucesan, L.A. Kendall, An analytic mechanistic cutting force model for milling operations: a theory and methodology, *Trans ASME J Eng Ind* 116 (1994) 324–330.
- [15] J.H. Ko, W.S. Yun, D.W. Cho, K.F. Ehmman, Development of a virtual machining system—Part I: approximation of the size effect for cutting force prediction, *Int J Mach Tools Manuf* 42 (2002) 1595–1605.
- [16] J.H. Ko, D.W. Cho, 3D ball-end milling force model using instantaneous cutting force coefficients, *Trans ASME J Manuf Sci Eng* 127 (2005) 1–12.
- [17] Wan M, Zhang WH, Qin GH, Tan G. Efficient calibration of instantaneous cutting force coefficients and runout parameters for general end mills. *Int J Mach Tools Manuf*, (2006), doi:10.1016/j.ijmactools.2006.06.012.
- [18] W.S. Yun, D.W. Cho, An improved method for the determination of 3D cutting force coefficients and runout parameters in end milling, *Int J Adv Manuf Technol* 16 (2000) 851–858.
- [19] W.A. Kline, R.E. DeVor, The effect of runout on cutting geometry and forces in end milling, *Int J Mach Tool Des Res* 23 (1983) 123–140.
- [20] M. Wan, W.H. Zhang, Calculations of chip thickness and cutting forces in flexible end milling, *Int J Adv Manuf Technol* 29 (2006) 637–647.
- [21] J.-J.J. Wang, S.Y. Liang, Chip load kinematics in milling with radial cutter runout, *Trans ASME J Eng Ind* 118 (1996) 111–116.
- [22] A. Azeem, H.Y. Feng, L.H. Wang, Simplified and efficient calibration of a mechanistic cutting force model for ball-end milling, *Int J Mach Tools Manuf* 44 (2004) 291–298.